Multiple spatiotemporal modes of actin reorganization by NMDA receptors and voltage-gated Ca^{2+} channels

Tomoyuki Furuyashiki*, Yoshiki Arakawa*, Sayaka Takemoto-Kimura*, Haruhiko Bito*†‡, and Shuh Narumiya*

*Department of Pharmacology, Kyoto University Faculty of Medicine, and †Precursory Research for Embryonic Science and Technology, Japan Science and Technology Corporation, Sakyo-ku, Kyoto 606-8315, Japan

Edited by Richard W. Tsien, Stanford University School of Medicine, Stanford, CA, and approved August 22, 2002 (received for review March 14, 2002)

Cytoskeleton is believed to contribute to activity-dependent processes underlying neuronal plasticity, such as regulations of cellular morphology and localization of signaling proteins. However, how neuronal activity controls actin cytoskeleton remains obscure. Taking advantage of confocal imaging of enhanced GFP-actin in the primary culture of hippocampal neurons, we show that synaptic activity induces multiple types of actin reorganization, both at the spines and at the somatic periphery. Activation of *N*-methyl-D-aspartate receptors, accompanied with a local rise in $[Ca^{2+}]i$, was sufficient to trigger a slow and sustained recruitment of actin into dendritic spines. In contrast, opening of voltage-gated Ca^{2+} channels rapidly and reversibly enhanced cortical actin at the somatic periphery but not in the spines, in keeping with a high transient rise in somatic $[Ca^{2+}]i$. These data suggest that spatiotemporal dynamics of $[Ca^{2+}]i$, triggered by activation of *N*-methyl-D-aspartate receptors and voltage-gated Ca^{2+} channels, provides the molecular basis for activity-dependent actin remodeling.

Establishment and remodeling of neural connections require a spatially and temporally orchestrated control of neuronal morphology (1, 2) and fine-tuning of assemblies of signaling complexes (3–8). Although such dynamic reorganization is common during embryonic development, recent evidence indicated that, even in mature brain tissues, neuronal activity may initiate and regulate the active modification of cell shape (9–15) and the sorting of neuronal molecules (16–19). *In vitro* studies suggest the requirement for an actin-based mechanism in dendritic spine motility (20, 21) as well as in localization of synaptic proteins at the postsynaptic density (22). These lines of evidence indicate the importance of cytoskeletal signaling in regulating neuronal properties even after their functional maturation.

Despite a growing interest in the role of actin remodeling during activity-dependent modification of neuronal properties, the fundamental question as to how neuronal activity regulates actin filaments has not been settled. For instance, neuronal activity has been associated with either an increase (9, 11, 14, 15) or a decrease (10, 13) in the number of dendritic spines. Furthermore, intracellular Ca^{2+} rise seemed to give rise to opposite effects on actin cytoskeleton. Ca^{2+}-dependent accumulation of actin has been reported in goldfish retinal bipolar cells (23) and in developing grasshopper neurons (24), whereas others have found an *N*-methyl-D-aspartate (NMDA)-stimulated actin dislocation at dendritic spines (25, 26). These apparently conflicting observations raise the possibility that activity-dependent regulation of actin reorganization may be ruled by multiple coexisting modes of signaling from synapse to cytoskeleton.

Setting aside such controversy, most studies have similarly argued that intracellular Ca^{2+} is involved in actin reorganization (23–27). Recent pharmacological evidence has highlighted the diversity of Ca^{2+} entry sources, each of which may have distinct functions in various cellular phenomena, such as synaptic plasticity (for review, see ref. 4) and gene expression (28). Previous work on Ca^{2+}-induced actin responses indeed used various kinds of stimulation protocols which were likely to activate distinct routes of Ca^{2+} entry. Thus, the reported dichotomy in Ca^{2+}-mediated actin responses might reflect the functional segregation of different Ca^{2+} sources, each contributing distinctly during actin reorganization. To gain definitive insights into these issues, we visualized directly actin dynamics in live, synaptically connected, cultured hippocampal neurons by use of enhanced GFP (EGFP)-actin and analyzed Ca^{2+}-based mechanisms in activity-dependent actin reorganization.

Materials and Methods

Construction of the adenovirus which expresses EGFP-actin, the primary culture of hippocampal neurons, adenoviral infection, pharmacological and electrical stimulations, imaging of EGFP-actin and vital fluorescent dyes (FM4–64, Fluo-4/AM, and Fura-2/AM), digital processing of these fluorescent images, and statistical data analyses were performed as described with minor modifications. The detailed information about these experimental procedures is provided in *Additional Text About Materials and Methods*, which is published as supporting information on the PNAS web site, www.pnas.org. All images were acquired at room temperature in Tyrode solution supplemented with appropriate drugs. All fluorescence values of EGFP-actin had been normalized to their prestimulus values before they were subjected to the quantitative analyses. The distinction between different actin structures (the punctate and the cortical accumulations) was determined according to their shapes and sizes (see *Additional Text* in supporting information). In the ratiometric Ca^{2+} imaging experiments, we included 5 μM ω-conotoxin MVIIC during all stimulations to remove the contamination of presynaptic Ca^{2+} transients triggered by opening of N- or P/Q-type Ca^{2+} channels and because bath application of Cd^{2+} significantly quenched Fura-2 fluorescence. This manipulation by itself did not affect actin dynamics induced by high K^+.

Results

Synaptic Activity Induced Multiple Types of Actin Reorganization at Distinct Subcellular Sites. To introduce EGFP-actin to synaptically connected cultured hippocampal neurons with minimal toxicity, we constructed an adenovirus which expresses EGFP-actin (for the detailed characterization of EGFP-actin properties, see Fig. 6, which is published as supporting information on the PNAS web site). EGFP-actin was localized to dendritic spines (see Fig. 7, which is published as supporting information on the PNAS web site), in close agreement with reports of endogenous actin molecules (29, 30). Furthermore, synapses and dendritic spines were formed intact in the presence of EGFP-actin (data not

This paper was submitted directly (Track II) to the PNAS office.

Abbreviations: EGFP, enhanced GFP; VGCCs, voltage-gated Ca^{2+} channels; NMDA, *N*-methyl-D-aspartate; ROI, region of interest.

‡To whom correspondence should be addressed. E-mail: hbito@mfour.med.kyoto-u.ac.jp.

 www.pnas.org/cgi/doi/10.1073/pnas.212148999

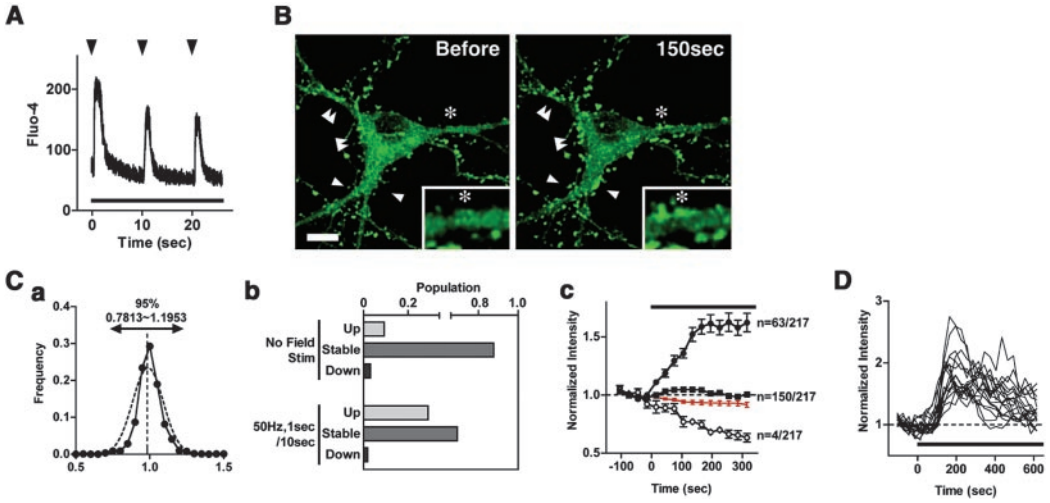

Fig. 1. Electrically patterned synaptic activity induces enhancement of actin puncta in spine-like structures. (*A*) The fluorescence intensity of Fluo-4 in a neuronal cell body was measured in the line-scan mode. Trains at 9-s intervals (arrowheads) were continuously applied by using field stimulation electrodes throughout the duration of the recording (bar). (*B*) Significant numbers of punctate accumulation of EGFP-actin (arrowheads) were detected at the 150-s time point during the same stimulus train as in *A*. The magnified and smoothed image is shown in *Inset*. **, same position. (Bar = 10 μm.) See also Movie 1. (*Ca*) Distribution of basal EGFP-actin fluorescence (solid line) and its Gaussian-fitted curve (dotted line). EGFP-actin fluorescence intensity was normalized to average intensity. Ninety-five percent of puncta were included in the 0.7813–1.1953 interval (mean ± 2 SD). (*Cb*) Electrical field stimulation augments the number of puncta with a fluorescence increase greater to 2 SD (''Up'', >1.1953-fold of the mean) while diminishing the number of puncta with a lesser increase (''Stable'', changes smaller than 2 SD; ''Down'', decrease greater than 2 SD). Two hundred and seventeen puncta from 8 stimulated neurons and 65 puncta from 4 unstimulated neurons were analyzed. (*Cc*) Temporal profiles of averaged fluorescence intensity in the three categories (''Up'', ●; ''Stable'', ■; ''Down'', ○). The total integrated fluorescence from all pixels in the soma area is also shown (red line). (*D*) Individual traces of EGFP-actin fluorescence from 18 puncta showing fluorescence increase (>SD) in a single representative neuron. The same stimulus as in *A* was applied (bar). Data are shown as means ± SEM.

shown). These data verified EGFP-actin as a suitable tracer of endogenous actin molecules.

Taking advantage of confocal time-lapse imaging of EGFP-actin expressed in cultured hippocampal neurons, we asked whether and how actin dynamics are controlled by synaptic activity. First, we applied continuous trains of electrical pulses to trigger synaptic activity by means of extracellular field stimulation. However, a train of electrical pulses delivered at even as high as 50 Hz was unable to induce a detectable change in actin localization (data not shown). Based on Ca^{2+} imaging, we suspected that the failure of EGFP-actin response might be caused by the lack of sustained increase in $[Ca^{2+}]i$ during prolonged application of continuous electrical trains. After optimization of stimulus patterns for the maximal Ca^{2+} increase, we found that bursts of 50-Hz, 1-s stimuli delivered continuously at 9-s intervals (Fig. 1*A*) elicited reliable changes in punctate EGFP-actin signals, most likely at dendritic spines, when given after 12-h pretreatment with tetrodotoxin (TTX) followed by its washout (15 of 23 neurons; Fig. 1*B*; 18 ± 3% increase from baseline at 315 s after the initiation of the stimulus in 8 neurons; $P < 0.0001$; see Fig. 8*A* and Movie 1, which are published as supporting information on the PNAS web site). In contrast, little change was detected in nonstimulated control neurons (3 ± 5% increase at the same time point above, $P > 0.5$). It should also be noted that the distribution of EGFP fluorescence was not altered throughout field stimulation in cultured hippocampal neurons expressing EGFP (5 neurons, Fig. 8*B*). Thus, the recorded events were unlikely to be artifacts caused by cell toxicity, photodamage, or local modification of EGFP fluorescence property.

To examine the spine-to-spine variability in the activity-induced actin response, we compared the temporal profile of the fluorescence changes for each EGFP-actin puncta following the stimulation above. The basal fluctuation of fluorescence values of individual puncta was well fitted with a single Gaussian (Fig. 1*Ca*); a two-fold standard deviation (SD) was used as a threshold to assess the statistical significance of stimulus-dependent changes. In the absence of stimuli, the fluorescence values changed little, with few puncta showing a change in fluorescence exceeding 2 SD (9.2%, Fig. 1*Cb*, upper half). In contrast, when a 50-Hz, 1-s burst field stimulation was applied every 10 s, about 30% of the puncta revealed a fluorescence increase exceeding 2 SD (29%; Fig. 1*Cb*, lower half and Fig. 1*Cc*). The change in fluorescence properties of EGFP itself was negligible as the total sum of fluorescence in the soma varied little (8 ± 2% decrease

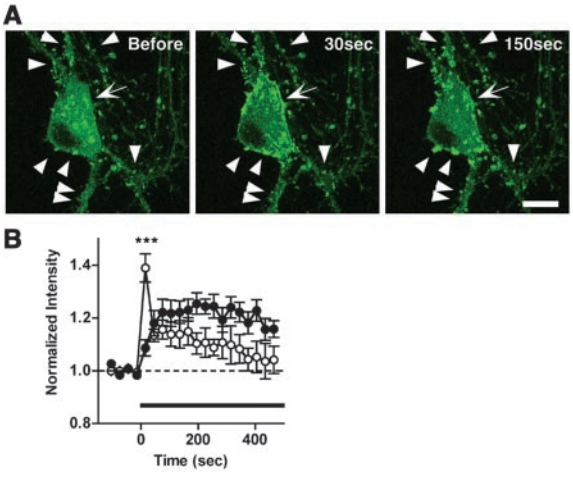

Fig. 2. Rapid induction and decay of cortical actin enhancement is also triggered by patterned synaptic activity. (*A*) A representative neuron showing both cortical (arrow) and punctate (arrowheads) accumulations of EGFP-actin. (Bar = 10 μm.) (*B*) Punctate (●, 16 ROIs from 2 neurons) and cortical (○, 9 ROIs from 2 neurons) actin accumulations revealed a striking difference in activation and decay kinetics during the whole duration of the field stimulation (shown by bar). All data are shown as means ± SEM. ***, $P < 0.001$.

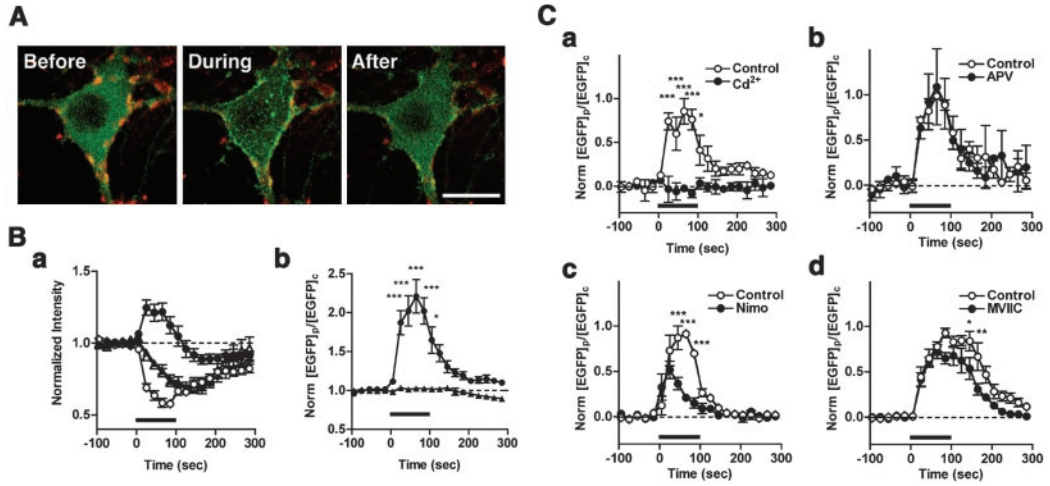

Fig. 3. High K^+-induced depolarization elicited rapid and reversible accumulation of EGFP-actin to the somatic periphery through the opening of voltage-gated Ca^{2+} channels. (*A*) EGFP-actin (green) distribution before, during, and after depolarization with 90 mM K^+ in a hippocampal neuron, with a simultaneous recording of the decay of FM4–64 signals (red). See also Movie 2. (Bar = 15 μm.) (*Ba*) Traces of EGFP-actin (13 neurons, ● and ○) or EGFP (4 neurons, ▲ and △) intensity at the somatic periphery (the single brightest ROI at the edge of the EGFP-actin signals at the soma, ● and ▲) and the bulk cytoplasm (the single darkest ROI at the perinuclear region, ○ and △). (*b*) The ratio of the fluorescence intensity at the somatic periphery and the bulk cytoplasm ([EGFP]p/[EGFP]c), normalized to the value before stimulation, as the translocation index for EGFP signals (●, EGFP-actin; ▲, EGFP). (*C a–d*) The dependence of high K^+-induced increases in [EGFP]p/[EGFP]c on various Ca^{2+} influx sources was examined in the absence (○) or presence (●) of various reagents such as 100 μM Cd^{2+} (*a*, 4 neurons), 50 μM D-APV (*b*, 3 neurons), 10 μM nimodipine (*c*, 3 neurons), or 5 μM ω-conotoxin MVIIC (*d*, 4 neurons). All data were rescaled based on the peak value during the control depolarization (○), applied 10 min before the second depolarization in the presence of the reagents (●). Repeated depolarization reliably induced the cortical actin accumulation (data not shown). Stimulus duration was shown by bar for each dataset. *, $P < 0.05$; **, $P < 0.01$; ***, $P < 0.001$. All of the plots are shown in means ± SEM.

at 315 s after the beginning of the stimulus; Fig. 1*Cc*, red line). Thus, synaptic stimulation induced a slow and sustained enhancement of EGFP-actin fluorescence in many, but not all, dendritic spines. Superimposed individual fluorescence profiles from one neuron, whose increase exceeded 1 SD, are shown in Fig. 1*D*. A relative synchrony in the rising time was observed across many spines within the same neuron during the initial accumulation phase. In contrast, a greater variability seemed to exist for the decay kinetics across different puncta. This seems to be caused, at least in part, by the fact that a small subgroup of puncta showed a sustained enhancement throughout the observation period, whereas most of the punctate accumulations gradually decayed to their original level.

In addition to the punctate accumulation, the brightness of EGFP-actin also significantly augmented at the somatic periphery (9 of 23 neurons, Fig. 2*A*). Interestingly, in six neurons, a rise in EGFP-actin signals also was found in dendritic spines in parallel with an increase in the cortical signals, allowing direct comparison of the kinetics between these two types of actin accumulation. Both the accumulation phase and the decay phase occurred significantly faster for the cortical actin than for the punctate enhancement (Fig. 2*B*). Such diversity in the temporal and spatial patterns of actin relocation is most consistent with the presence of multiple modes of activity-dependent actin reorganization within a single neuron.

Voltage-Gated Ca^{2+} Channels, but Not NMDA Receptors, Are Essential for Actin Accumulation to the Somatic Periphery. To determine what kind of synaptic activity directly triggers actin relocation, we examined the contribution of various Ca^{2+} entry sources. Massive depolarization was first applied by increasing the extracellular K^+ concentration from 5 mM to 90 mM (high K^+). As shown in Fig. 3 *A* and *B* (see also Movie 2, which is published as supporting information on the PNAS web site), this stimulus induced a rapid decrease in the diffuse cytoplasmic EGFP-actin signal in the soma, whereas a robust concentration of EGFP-actin was observed at the cell periphery. The latter change was reminiscent of the cortical accumulation induced by field stimulation. Such complementary changes in cytoplasmic and peripheral EGFP-actin signals indicate that actin massively relocated from the bulk cytoplasm to the cell periphery. These changes persisted throughout the duration of the depolarization, and were reversed upon its cessation (Fig. 3 *A* and *B*). By using [EGFP]p/[EGFP]c (see the legend of Fig. 3*Bb*) as an index for high K^+-induced actin relocation, the half-rising time of activation was found to be less than 30 s, whereas the half-decay time constant was on the order of 1 min (Fig. 3*Bb*). Acquisition of vertically sliced images revealed that high K^+ induced a linear enhancement of EGFP-actin signals at the lateral side but not at the top or at the bottom of the soma (Fig. 9, which is published as supporting information on the PNAS web site). In EGFP-expressing neurons, the same stimulus caused a uniform rate of decrease in the fluorescence signals at the somatic periphery and the cytoplasm (Fig. 3*Ba*), thus keeping the ratio of [EGFP]p/[EGFP]c constant (Fig. 3*Bb*).

Because removal of extracellular Ca^{2+} eliminated high K^+-induced actin relocation as determined under live or fixed conditions (data not shown), we next tested the specific contribution of several Ca^{2+} entry sources. Blockade of high voltage-activated (HVA) Ca^{2+} channels using Cd^{2+} (100 μM) abolished the cortical accumulation of EGFP-actin signals (Fig. 3*Ca*: 104% reduction from the control at 25 s after initiation of the stimulus, $P < 0.001$). In contrast, inhibition of NMDA receptors using D-APV (50 μM) had no significant effect (Fig. 3*Cb*: 12% reduction from the control at 25 s after initiation of the stimulus, $P > 0.05$). These data implied that Ca^{2+} entry through VGCCs may be critical for actin relocation induced by high K^+, whereas they failed to support a role of NMDA receptors in these processes. In keeping with this idea, nimodipine, a selective blocker for L-type VGCC, significantly blocked the maintenance phase of actin relocation (Fig. 3*Cc*; 78% reduction from the control at 85 s, $P < 0.001$), but not its initiation phase (Fig. 3*Cc*: 30% reduction from the control at 25 s, $P > 0.05$). In contrast, ω-conotoxin MVIIC at a dose known to inhibit N- and P/Q-type Ca^{2+} channels had a marginal effect on either phase (Fig. 3*Cd*:

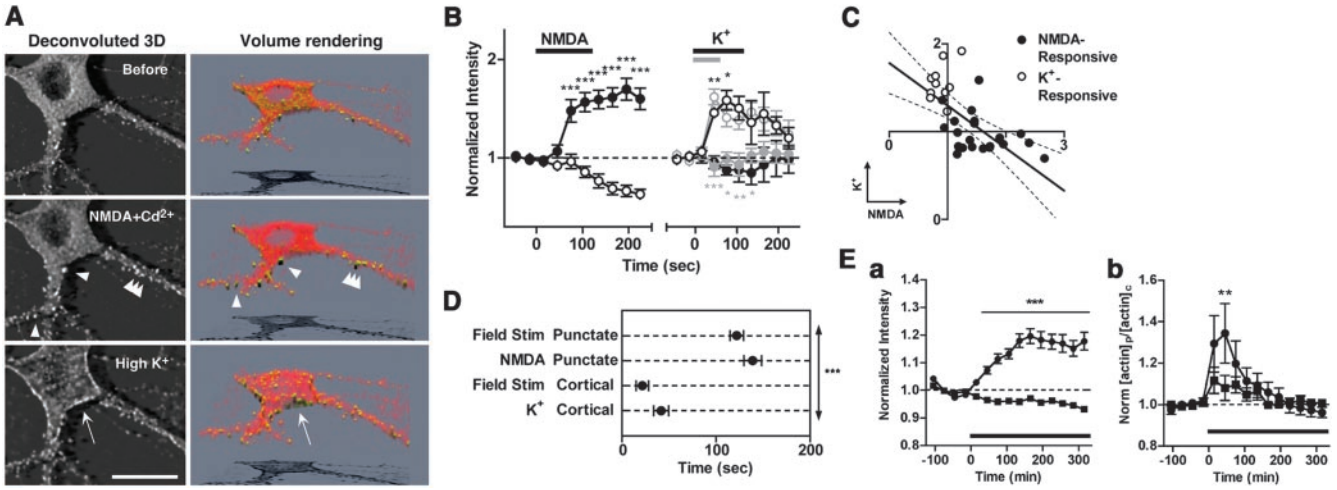

Fig. 4. Activation of NMDA receptors induced actin accumulation to the dendritic spines, but not to the somatic periphery. (*A Left*) Deconvoluted 3-D images of typical EGFP-actin distribution within the same hippocampal neuron, before (Before), after NMDA application with Cd^{2+} (NMDA+Cd^{2+}), and after a subsequent high K^+ depolarization following washout of NMDA and Cd^{2+} (High K^+). See also Movie 3. (Bar = 20 μm.) (*A Right*) A 3-D-rendered pseudocolor illustration of the distribution of NMDA-induced and high K^+-induced EGFP-actin accumulations in the panels at *Left*. EGFP-actin-enriched structures are illustrated in yellow; they are based on the arbitrary threshold (arrowheads and an arrow). The signals of EGFP-actin below the threshold are shown in red. (*B*) Temporal profiles of averaged EGFP-actin fluorescence at typical NMDA-responsive (●, 22 ROIs from 3 neurons) or high K^+-responsive (○, 10 ROIs from 3 neurons) regions. An increase exceeding 2 SD was considered as a significant response. High K^+ did not alter the fluorescence intensity at EGFP-actin puncta, irrespective of the stimulus duration (2 min, black, 1 neuron; 1 min, gray, 2 neurons). (*C*) Correlative plots of each individual ROI in *B*. Increases in EGFP-actin fluorescence during stimulation with NMDA (at 105 s) and with high K^+ (at 45 s) at either the NMDA-responsive or the high K^+-responsive regions are compared. Note that there are two distinct clusters with different responsiveness toward each stimulus. The responsiveness to NMDA and to high K^+ shows a negative correlation (slope of linear regression = -0.4855 ± 0.1181, $P < 0.001$, F test). The dotted line shows a 95% confidence interval for linear regression. (*D*) Averaged 0–80% rising times ($\tau_{0.8}$) are calculated and compared for the cortical and punctate actin accumulations induced by field stimulation and for NMDA- and high K^+-stimulation. (*E*) The punctate actin accumulation (*a*) was abolished in the presence of D-APV (50 μM or 100 μM, ■, 150 puncta from 10 neurons; ●, control trace). The cortical accumulation (*b*), which is quantified in the translocation index of [EGFP]p/[EGFP]c as in Fig. 3, was still induced by field stimulation in the presence of D-APV, although to a significantly lesser degree [11 neurons each with (■) or without (●) D-APV]. Data is shown as means ± SEM. *, $P < 0.05$; **, $P < 0.01$; ***, $P < 0.001$. Bars indicate stimulus duration.

7 and 30% decrease at 25 and 85 s, respectively, $P > 0.05$). These results are consistent with the involvement of multiple types of HVA Ca^{2+} channels in high K^+-induced cortical actin accumulation.

Activation of NMDA Receptors Induces Local Changes in Actin at the Spines but Not at the Somatic Periphery. At the hippocampal CA1 excitatory synapses, glutamatergic synaptic inputs induce significant amount of Ca^{2+} influx via NMDA receptors (31–33). It also has been shown that local electrical stimulation induces NMDA receptor-dependent changes in dendritic morphology (11, 14). We asked whether actin redistribution could be elicited by activation of NMDA receptors themselves, and thus stimulated the neurons with 100 μM NMDA in Mg^{2+}-free solution containing Cd^{2+} (100 μM; NMDA+Cd^{2+}). After preincubation with TTX, stimulation of NMDA receptors for a few minutes induced a prominent increase in the EGFP-actin fluorescence intensity in a significant proportion of synaptic puncta (Fig. 4*A*, arrowheads; see also Fig. 10 and Movie 3, which are published as supporting information on the PNAS web site) juxtaposed to FM4–64-positive spots (Fig. 11, which is published as supporting information on the PNAS web site). This result seems to be in contrast to the previous studies suggesting NMDA-induced actin depolymerization at dendritic spines (25, 26). However, it should be noted that, unlike in these previous articles, we completely blocked HVA Ca^{2+} channels to achieve pure NMDA stimulation. Although a number of puncta also showed an activity-dependent decrease in fluorescence (Fig. 10*B*), the decrease was comparable to the general loss of fluorescence from the cell soma (red line in Fig. 10*B*; $P > 0.05$ at any time point).

We next sequentially stimulated the same neurons with NMDA+Cd^{2+} and then with high K^+. As described above, initial stimulation with NMDA+Cd^{2+} induced a punctate accumulation of EGFP-actin signals in the spines (Fig. 4 *A* and *B*). After removal of NMDA and a 10-min washout, the punctate accumulation disappeared (Fig. 11). Even after the washout of Cd^{2+}, application of high K^+ failed to elicit the punctate accumulation previously induced by NMDA (Fig. 4 *A* and *B*). Instead, robust appearance of the cortical EGFP-actin accumulation was observed (Fig. 4*A*, arrow). The correlative plot of the fluorescence increase at individual spots upon NMDA and high K^+ stimuli further confirmed the specificity of the type of stimuli that potently trigger actin accumulation on a given local area (Fig. 4*C*). A similar result was obtained when the order of the stimuli was reversed (data not shown, 2 neurons) or when actin relocation was determined by immunostaining on fixed samples (Fig. 12, which is published as supporting information on the PNAS web site).

To compare the appearance of several types of activity-induced actin enhancement, we carried out quantitative analyses of accumulation kinetics after each kind of stimuli. NMDA+Cd^{2+} induced punctate accumulation with a time constant of 0–80% rise ($\tau_{0.8}$) of about 2 min (139 ± 9 s), whereas $\tau_{0.8}$ for high K^+ was about 40 s (42 ± 8 s, Fig. 4*D*). These time constants were comparable to $\tau_{0.8}$ of the punctate actin accumulation (122 ± 7 s) and that of the cortical actin accumulation (22 ± 7 s) during field stimulation, respectively. These data indicated the specific requirement of distinct Ca^{2+} sources for each type of synaptically induced actin structures. Indeed, D-APV strongly inhibited the punctate actin accumulation induced by field stimulation, whereas the cortical accumulation could still be induced in the presence of D-APV, although to a significantly lower degree (Fig. 4*E*). Therefore, Ca^{2+} entry via HVA Ca^{2+} channels and NMDA receptors is likely to cause distinct and complementary patterns of actin relocation upon synaptic stimulation.

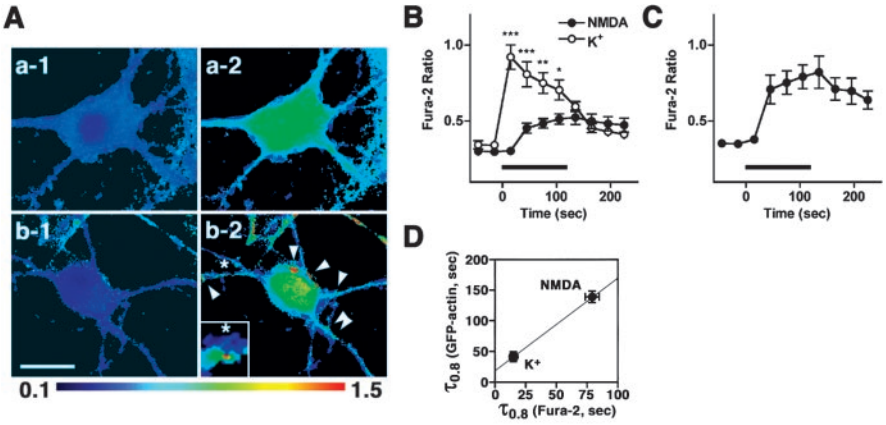

Fig. 5. Spatial and temporal Ca^{2+} dynamics is tightly linked with activity-dependent actin reorganization following high K^+ and NMDA-stimuli. (*A*) Ratiometric measurements of Fura-2 fluorescence excited at 340 nm and at 380 nm before (*a-1*, *b-1*) and at 105 s during stimuli (*a-2*, *b-2*) in neurons stimulated with high K^+ (*a*), and in those stimulated with NMDA in the absence of Mg^{2+} and in the presence of nimodipine (*b*). All Ca^{2+} imaging was performed in the presence of 5 μM ω-conotoxin MVIIC to avoid the contamination of large Ca^{2+} increase at presynaptic terminals. Localized Ca^{2+} transients (*b-2*, white arrowheads) were observed only in NMDA-stimulated cells. Stimulus duration was 2 min for each stimulus. A magnified and smoothed view of a typical local dendritic Ca^{2+} rise is shown in *Inset*. The asterisk in each image shows the same position. (*B*) Comparison of Ca^{2+} transients at the somatic periphery upon high K^+ (○, 4 neurons) or NMDA (●, 11 neurons) stimulation. Note the distinction in the amplitude and the kinetics of the two responses. (*C*) Slow but robust Ca^{2+} transients are induced at localized puncta in the dendrites and the soma upon NMDA activation—36 ROIs from 11 neurons. (*D*) Correlation between $\tau_{0.8}$ for induced Ca^{2+} transients and actin responses. Data are shown as means ± SEM. *, $P < 0.05$; **, $P < 0.01$; ***, $P < 0.001$. Bars indicate stimulus durations.

A Link Between Spatiotemporal Modulation of $[Ca^{2+}]i$ by NMDA Receptors and Voltage-Gated Ca^{2+} Channels and Activity-Dependent Actin Recruitment. Local control of Ca^{2+} dynamics provides a mechanism for tight regulation of actin behavior and actin-based contractility in smooth muscles (34), but this has not been tested fully in neurons. Thus, we tried to analyze whether distinct actin responsiveness toward NMDA receptors and VGCCs may be controlled directly by Ca^{2+} dynamics through these channels. Ratiometric Ca^{2+} imaging using Fura-2/AM-loaded neurons indicated that high K^+-stimulated hippocampal neurons underwent a massive and global, but reversible, rise in $[Ca^{2+}]i$ throughout the cell (Fig. 5 *Aa* and *B*). In contrast, NMDA application in the absence of Mg^{2+} and in the presence of nimodipine only resulted in a slower and smaller $[Ca^{2+}]i$ increase in most parts of the neurons, which persisted even after the cessation of the stimuli (Fig. 5 *Ab* and *B*). However, a large and sustained increase in $[Ca^{2+}]i$ was recorded as localized puncta on the dendrites and the soma (Fig. 5 *Ab-2* and *C*). The amplitude of this localized Ca^{2+} response ("Ca^{2+} hotspots") was comparable to that induced by high K^+ at the somatic periphery. These Ca^{2+} hotspots were induced in an NMDA-specific and stimulus-dependent manner (Fig. 5*A* and Fig. 13, which is published as supporting information on the PNAS web site).

To gain insight into the relationship between Ca^{2+} increase and EGFP-actin accumulation, $\tau_{0.8}$ for rise in $[Ca^{2+}]i$ and EGFP-actin fluorescence were compared. The global and rapid rise in $[Ca^{2+}]i$ induced by high K^+ occurred with $\tau_{0.8}$ of about 15 s (15 ± 0 s), coincident with the rapid initiation of the high K^+-induced cortical recruitment of actin ($\tau_{0.8}$ = 42 ± 8 s, Fig. 5*D*). In contrast, NMDA-induced rise in $[Ca^{2+}]i$ appeared with a significantly larger time constant ($\tau_{0.8}$ = 79 ± 6 s, $P < 0.0001$ compared with $\tau_{0.8}$ for high K-induced $[Ca^{2+}]i$ rise, Fig. 5*D*). The NMDA-induced EGFP-actin recruitment was initiated at the similar time constant as $[Ca^{2+}]i$ (Fig. 5*D*, $\tau_{0.8}$ = 139 ± 9 s). Therefore, an apparent correlation was observed between $\tau_{0.8}$ for $[Ca^{2+}]i$ mobilization and actin reorganization induced by either high K^+ or NMDA stimulus. Taken together, our data suggest that distinction in Ca^{2+} dynamics based on Ca^{2+} entry sources plays a dominant role in directing spatiotemporal patterns of activity-induced actin reorganization (Fig. 14, which is published as supporting information on the PNAS web site).

Discussion

Actin filaments are major components of the cytoskeleton at the postsynaptic sites of the excitatory synapses (29, 30). The bivalent nature of actin cytoskeleton dynamics, rigidity, and plasticity has attracted neurobiologists for decades as a possible molecular basis that may account for certain kinds of synaptic plasticity (30). In this study, we report three main observations concerning activity-induced actin responses in hippocampal neurons.

First, certain patterns of synaptic activity, triggered through extracellular field stimulation, induce actin accumulation at dendritic spines and at the somatic periphery as rapidly as in the order of minutes. It is noteworthy that maximal actin accumulation to dendritic spines could only be observed after prior silencing of endogenous neuronal activity (see the discussion in *Additional Text*), adding to the notion that activity-dependent actin regulation is highly dependent on the context in which a neuron receives synaptic inputs.

Second, spatiotemporal dynamics in $[Ca^{2+}]i$ triggered by either VGCCs or NMDA receptors is coupled with two separate types of activity-induced actin accumulations with regard to their onset kinetics (fast vs. slow), subcellular distribution (somatic periphery vs. dendritic spines), and duration (transient vs. persistent). The high correlation between the onset kinetics of actin accumulations and $[Ca^{2+}]i$ upon NMDA and high K^+ stimulation is consistent with the possibility that a uniform biochemical process is involved in the conversion of Ca^{2+} entry into actin recruitment. The fact that NMDA receptors are enriched at the synapse (for example, see ref. 19), whereas L-type VGCC is more diffusely distributed at the somatodendritic region (35) implies that the actin reorganizations in this study occurred at the subcellular loci physically close to Ca^{2+} entry sites. Thus, we favor the simplest view that Ca^{2+} influx through distinct types of Ca^{2+} entry channels locally activates actin regulatory mechanisms, resulting in a high correlation between the spatiotemporal properties of Ca^{2+} dynamics and actin reorganization. However, it should also be noticed that either punctate or cortical actin reorganization occurs at only a fraction of those regions expressing responsible Ca^{2+} entry channels. This result suggests that factors yet unrevealed may further contribute to the ultimate outcome of actin behaviors. Detailed analyses of actin regulatory mechanisms within each spine are necessary for elucidating fully

the molecular basis by which spatial distribution of actin reorganization is determined.

Third, we found that activity-induced actin accumulation is heterogeneous in nature across individual dendritic spines. This finding is supported by two observations. First, we observed that some, but not all, spines in a single neuron show an increase in actin content upon synaptic or NMDA-receptor activation (Fig. 1*C* and Fig. 10). Second, even across those spines where actin accumulation was recorded, there was considerable heterogeneity in the decay kinetics, such that the spine actin content was increased more persistently in some spines than in others (Fig. 1*D*). Therefore, it is likely that actin content could be separately controlled at the single-spine level. This view is consistent with a previous report suggesting that local elevation of intracellular Ca^{2+} leads to localized actin enhancement in grasshopper neurons (24). To clarify fully the independence of actin regulation at individual spines, local activation of excitatory synapses by use of local application of high K^+ or glutamate, with all neighboring synapses silenced, remains to be carried out.

In conclusion, we found that synaptic activity induces multiple modes of actin reorganization of discrete spatial and temporal patterns, each of which is driven by a distinct Ca^{2+} entry source. It highlights the notion that spatiotemporal control of actin reorganization is tightly coupled to complex patterns of synaptic inputs and underlying Ca^{2+} dynamics. Whether and how such specificity in Ca^{2+}-actin coupling could contribute to activity-dependent controls of spine morphology and protein localization underlying synaptic plasticity awaits future studies.

We thank Roger Y. Tsien (University of California at San Diego) and Atsushi Miyawaki (RIKEN-Brain Science Institute, Wako, Japan) for advice on GFP mutants; Hirohide Takebayashi (National Institute for Physiological Sciences, Okazaki, Japan) for technical advice on the adenovirus construction; Fumiyoshi Ishidate, Kazunori Sugai, and Shigeki Yokoyama (Carl Zeiss, Japan) for providing access to the HUYGENS SYSTEM V.2.1.7 (Scientific Volume Imaging, Hilversum, The Netherlands) and IMARIS V.2.7 (Bitplane, Zurich); Kimiko Nonomura for technical assistance; and Tae Arai and Hiroko Nose for secretarial help. This work was supported by Grants-in-Aid from the Ministry of Education, Culture, Sports, Science and Technology of Japan (to S.N. and H.B.) and the Ministry of Health of Japan (to H.B.), and Research Grants from the Asahi Glass Foundation, the Cell Science Research Foundation, the Nissan Science Foundation, the Tanabe Medical Frontier Conference, the Ube Research Foundation, the Yamanouchi Foundation for Research on Metabolic Disorders, and a Precursory Research for Embryonic Science and Technology investigatorship from the Japan Science and Technology Corporation (to H.B.). T.F. is a recipient of a pre- and postdoctoral fellowship from the Japan Society for the Promotion of Science.

1. Andersen, P. (1999) *Nature* **399,** 19–21.
2. Smith, S. J. (1999) *Science* **283,** 1860–1861.
3. Blackstone, C. & Sheng, M. (1999) *Cell Calcium* **26,** 181–192.
4. Bliss, T. V. & Collingridge, G. L. (1993) *Nature* **361,** 31–39.
5. Kennedy, M. B. (1998) *Brain Res. Brain Res. Rev.* **26,** 243–257.
6. Kim, J. H. & Huganir, R. L. (1999) *Curr. Opin. Cell Biol.* **11,** 248–254.
7. Ziff, E. B. (1997) *Neuron* **19,** 1163–1174.
8. Friedman, H. V., Bresler, T., Garner, C. C. & Ziv, N. E. (2000) *Neuron* **27,** 57–69.
9. Andersen, P. & Soleng, A. F. (1998) *Brain Res. Brain Res. Rev.* **26,** 353–359.
10. Dalva, M. B., Ghosh, A. & Shatz, C. J. (1994) *J. Neurosci.* **14,** 3588–3602.
11. Engert, F. & Bonhoeffer, T. (1999) *Nature* **399,** 66–70.
12. Hosokawa, T., Rusakov, D. A., Bliss, T. V. & Fine, A. (1995) *J. Neurosci.* **15,** 5560–5573.
13. Kirov, S. A. & Harris, K. M. (1999) *Nat. Neurosci.* **2,** 878–883.
14. Maletic-Savatic, M., Malinow, R. & Svoboda, K. (1999) *Science* **283,** 1923–1927.
15. Toni, N., Buchs, P. A., Nikonenko, I., Bron, C. R. & Muller, D. (1999) *Nature* **402,** 421–425.
16. Koh, Y. H., Popova, E., Thomas, U., Griffith, L. C. & Budnik, V. (1999) *Cell* **98,** 353–363.
17. Shen, K. & Meyer, T. (1999) *Science* **284,** 162–166.
18. Shi, S. H., Hayashi, Y., Petralia, R. S., Zaman, S. H., Wenthold, R. J., Svoboda, K. & Malinow, R. (1999) *Science* **284,** 1811–1816.
19. Rao, A. & Craig, A. M. (1997) *Neuron* **19,** 801–812.
20. Dunaevsky, A., Tashiro, A., Majewska, A., Mason, C. & Yuste, R. (1999) *Proc. Natl. Acad. Sci. USA* **96,** 13438–13443.
21. Fischer, M., Kaech, S., Knutti, D. & Matus, A. (1998) *Neuron* **20,** 847–854.
22. Allison, D. W., Gelfand, V. I., Spector, I. & Craig, A. M. (1998) *J. Neurosci.* **18,** 2423–2436.
23. Job, C. & Lagnado, L. (1998) *J. Cell Biol.* **143,** 1661–1672.
24. Lau, P. M., Zucker, R. S. & Bentley, D. (1999) *J. Cell Biol.* **145,** 1265–1275.
25. Furukawa, K., Fu, W., Li, Y., Witke, W., Kwiatkowski, D. J. & Mattson, M. P. (1997) *J. Neurosci.* **17,** 8178–8186.
26. Halpain, S., Hipolito, A. & Saffer, L. (1998) *J. Neurosci.* **18,** 9835–9844.
27. Colicos, M. A., Collins, B. E., Sailor, M. J. & Goda, Y. (2001) *Cell* **107,** 605–616.
28. Bito, H., Deisseroth, K. & Tsien, R. W. (1996) *Cell* **87,** 1203–1214.
29. Matus, A., Ackermann, M., Pehling, G., Byers, H. R. & Fujiwara, K. (1982) *Proc. Natl. Acad. Sci. USA* **79,** 7590–7594.
30. Fifkova, E. & Morales, M. (1992) *Int. Rev. Cytol.* **139,** 267–307.
31. Emptage, N., Bliss, T. V. & Fine, A. (1999) *Neuron* **22,** 115–124.
32. Schiller, J., Schiller, Y. & Clapham, D. E. (1998) *Nat. Neurosci.* **1,** 114–118.
33. Yuste, R., Majewska, A., Cash, S. S. & Denk, W. (1999) *J. Neurosci.* **19,** 1976–1987.
34. Somlyo, A. P. & Somlyo, A. V. (1994) *Nature* **372,** 231–236.
35. Hell, J. W., Westenbroek, R. E., Warner, C., Ahlijanian, M. K., Prystay, W., Gilbert, M. M., Snutch, T. P. & Catterall, W. A. (1993) *J. Cell Biol.* **123,** 949–962.